Acta Polytechnica **65**(4):478–492, 2025
https://doi.org/10.14311/AP.2025.65.0478

Published by the Czech Technical University in Prague

EFFECTS OF COUPLED DIFFUSION AND BUOYANCY FORCES ON THREE-DIMENSIONAL MHD CONVECTIVE WILLIAMSON-CASSON NANOFLUID FLOW: A NUMERICAL STUDY

Bhargavi Samudrala[a,*], K. Jayalakshmi[b], Murali Gundagani[c]

[a] *Joginpally B. R. Engineering College, 500075 Bhaskar Nagar, India*

[b] *Jawaharlal Nehru Technological University, 515002 Anantapuram, India*

[c] *Geethanjali College of Engineering and Technology, 501301 Cheeryal, India*

[*] corresponding author: bhargavi.mathematics@gmail.com

Abstract. The study analyses how thermal diffusion, Dufour effect, thermophoretic forces, Brownian motion, buoyancy-driven convection, and magnetic fields collectively impact microbial behaviour in a convective MHD flow of a Williamson-Casson nanofluid past an exponentially stretched surface. Utilising Boussinesq's approach, we examine the density fluctuations induced by temperature and concentration variations. Upon implementing convective surface boundary conditions for the sheet, the governing partial differential equations are transformed into ordinary differential equations and then resolved computationally using the MATLAB "bvp4c" method. This procedure is continued until the equations are resolved. The graphical representation illustrates the impact of essential flow parameters on temperature, concentration, main and secondary velocities, and microorganism profiles. To better understand the behaviour of these parameters, numerical calculations of the local Sherwood number, motile density, skin-friction coefficient, and Nusselt number are conducted. Tabular analysis is used to evaluate the impact of various parameters on fluid flow, including skin friction, the Nusselt number, motile density, and the Sherwood number. The data provided herein closely resemble those previously published by other authors. Ultimately, nanofluids have the potential for significant technical applications in the future. This is due to certain physical characteristics examined in this study. These attributes possess the capacity to enhance thermophysical characteristics and heat mass transport.

Keywords: MHD, three-dimensional, Williamson fluid, Casson fluid, nanofluid, exponentially stretching sheet, microorganisms, coupled diffusion, buoyancy forces, magnetic field.

1. Introduction

A stretched surface causes a boundary layer flow, which improves the mixing that occurs adjacent to the surface, hence increasing the amount of heat and mass that is transferred. The stretching motion enhances mixing and heat transfer in nanofluids, which contain nanoparticles that boost thermal conductivity, surpassing the performance of stationary surfaces. Stretching surfaces are widely used in many manufacturing processes, including extrusion, wire drawing, and glass production. These processes need to manage cooling and heat drainage in order to function properly. In addition, these surfaces are necessary for the analysis of flow dynamics and the improvement of industrial business processes. Within the realm of microfluidic and cooling systems, the incorporation of nanofluids and stretched surfaces has the potential to significantly improve thermal management. Subsequent research such as that conducted by Reddy et al. [1] and Hussanan et al. [2] focused on the magnetohydrodynamic (MHD) flow and heat transmission of nanofluids over stretched surfaces. These studies provided substantial insight into heat generation and boundary conditions. Mahanthesh et al. [3] and Tulu et al. [4] investigated the flow behaviour of SWCNT and MWCNT nano-liquids over spinning surfaces and assessed the influence of heat sources. Both groups of researchers reached comparable results. The mixed convective flow of carbon nanotubes with Newtonian heating over a stretched cylinder was investigated by Muhammad and Hayat [5]. A thorough investigation was carried out by Shah et al. [6] with the purpose of increasing the entropy of nanofluid flow of fourth-grade over a deformable Riga wall. There was an investigation conducted by Salamah Aljaloud and colleagues [7] into the flow of pair stress nanofluid that was caused by a stretched surface. The researchers looked at the effects of an induced magnetic field as well as the effects of variable thermal conductivity. An investigation was conducted by Amjad and colleagues [8] to determine the effects of the Lorentz force and an induced magnetic field on the flow of Casson micropolar nanofluid over a permeable curved stretching or shrinking surface that is located inside a stagnation region. The nonlinear dissipative slip flow of Jeffrey nanomaterial across a curved surface was explored by Khan and Alzahrani [9]. This investigation included the formation of entropy as well

as the acquisition of activation energy. A research investigating the transmission of heat in magnetohydrodynamic flow over a flexible Riga wall was carried out by Shah et al. [10], who took into consideration the rate at which entropy was produced. Over the course of their research, Othman and colleagues [11] looked into the magnetohydrodynamic stagnation point in nanofluid flow as well as the heat transfer of carbon nanotubes on a decreasing surface that had a heat-sink characteristic. An investigation of the magnetohydrodynamic behaviour of carbon nanotubes was carried out by Majeed et al. [12] in the flow of a rotating nanofluid over a stretched surface that was permeable. Within the context of magnetohydrodynamics, Samat et al. [13] conducted an investigation on the flow and heat transfer of carbon nanotube nanofluids over a moving surface. An investigation of the Darcy-Forchheimer flow of hydromagnetic nanofluid over a stretching/shrinking sheet inside a thermally stratified porous medium was carried out by Ganesh et al. [14]. This investigation included investigation into the impacts of second-order slip, viscosity, and Ohmic dissipation. Jawad et al. [15] conducted an investigation of the Darcy-Forchheimer flow of Maxwell nanofluid over a porous stretched sheet. They used Arrhenius activation energy and Nield boundary conditions in their investigation.

Bioconvection in nanofluids has been the subject of a significant amount of research in recent years. This is due to the fact that nanofluids are used in biomedical applications, microbial transport, and refrigeration technologies that are more effective. The process of bioconvection occurs when the density and flow patterns of a fluid are altered by the presence of microorganisms that are moving. The complicated fluid behaviour that these systems exhibit is influenced by the interactions that take place between the base fluid, nanoparticles, and microbes all working together. Because they make use of nanofluids, which are nanoparticle suspensions that enhance thermal and mass transport properties, this is the reason why they are successful. When it comes to nanofluids, researchers have investigated a wide range of characteristics that influence bioconvection. These parameters include external pressures, stability limitations, temperature effects, and solutal effects. Agarwal et al. [16] conducted research on the thermally radiative flow of Powell-Eyring nanofluid. Their findings shed light on the impacts of swimming microorganisms and viscous dissipation. Choudhary et al. [17] conducted research to determine the effects of an unsteady magnetohydrodynamic hybrid nanofluid on a nonlinear stretchable porous sheet that was exposed to heat radiation and gyrotactic microorganisms. In their study [18], Rana and Basavarajappa investigated the dynamics of bioconvection in cone-disk systems that were either spinning or stationary. The flow of nano-bioconvective fluid on a vertical plate that was subjected to the effect of a magnetic field was investigated by Moradi et al. [19]. An investigation of radiative heat transfer was carried out by Algehyne and colleagues [20] in a magneto-bioconvection Maxwell fluid that was moving over a spinning disk. Khan et al. [21] explored the unsteady magnetohydrodynamic bio-convective flow of viscous nanofluid across a stretched surface. Wu et al. [22] investigated the entropy generation in the radiative motion of tangent hyperbolic nanofluid affected by gyrotactic microorganisms and activation energy. Both of these studies were conducted in the United States. In their study, Chaudhry and colleagues [23] looked into a mathematical model of a nanofluid flow via a stagnation point. The model included elements such as heat radiation, activation energy, and living organisms. For the purpose of analysing the swimming behaviour of motile microorganisms in bio-convection Casson nanofluid flow on a revolving circular disk, Mishra et al. [24] used the spectral quasi-linearisation approach. An investigation was conducted by Aboel and colleagues [25] to determine the effect that heat radiation and activation energy have on the flow of Casson nanofluid that demonstrates bioconvection and microorganisms over a disk. Within the framework of homogeneous-heterogeneous chemical processes, Khan et al. [26] conducted an investigation into the phenomenon of bio-convection in a Casson nanoliquid film that was extended onto a stretched cylinder. Through the use of the Cattaneo-Christov heat and mass flux theory, Khan et al. [27] conducted an investigation on the impact that the Hall current effect has on the bioconvection of Oldroyd-B nanofluid flow in a porous medium. An investigation of a gyrotactic mixed bioconvection flow of a nanofluid over a circular cylinder under convective boundary conditions was carried out by Rashad and Nabwey [28]. An MHD bioconvection flow and heat transfer of nanofluid via an exponentially stretchable sheet were the subjects of an investigation conducted by Ferdows et al. [29]. The flow of magneto-Carreau nanofluid via an inclined cylinder was investigated by Nabwey et al. [30], who investigated the effects of bioconvection and chemical reaction on the flow mechanisms. These studies, combined with the extensive research outlined in [31–49] form a strong basis for the current investigation.

This study conducts a quantitative analysis of a magnetohydrodynamic (MHD) flow involving a Williamson-Casson nanofluid across a stretching surface, considering the impact of buoyancy forces, coupled diffusion, and gyrotactic microorganisms. Building on prior research, the proposed model introduces innovative terms that set it apart from existing frameworks. A notable advancement is the integration of motile microorganisms into the traditional MHD nanofluid model, which introduces biological dynamics and alters the flow behaviour. The interplay between diffusion and buoyancy effects plays a critical role in shaping fluid dynamics, providing valuable insights into the intricate multi-physical interactions at play. The study employs partial differential equations

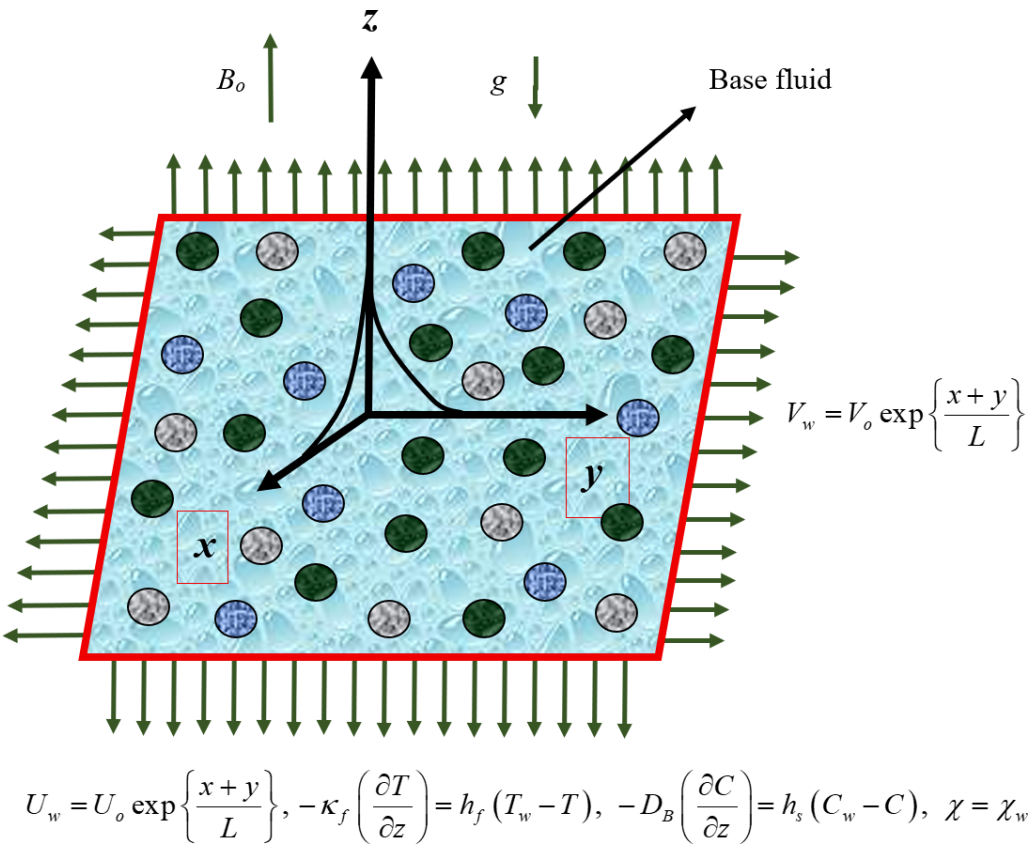

FIGURE 1. Schematic modelling of nanoparticle-infused casson fluid motion.

(PDEs) to model primary and secondary velocities, temperature, nanoparticle concentration, and microorganism density in bioconvective nanofluid flow over a stretching surface. Numerical solutions are derived using MATLAB's bvp4c solver. Key research questions include:

- The impact of magnetic fields on velocity profiles.
- The influence of Prandtl number, Brownian motion, Dufour effect, and thermophoresis on thermal behaviour.
- The role of Soret number, Lewis number, Brownian motion, and thermophoresis in mass transfer.
- How bioconvective Peclet and Lewis numbers affect microorganism distribution.
- Validation of numerical results against existing literature.

2. FLOW GOVERNING EQUATIONS

The joint effects of coupled diffusion effects (thermal diffusion (Soret) and diffusion thermo (Dufour)) on steady, electrically conducting, incompressible, MHD, three-dimensional flow of Williamson-Casson-Nanofluid by a linearly exponentially stretching sheet in the presence of Buoyancy forces, Brownian motion, and thermophoresis were studied using numerical solutions. The geometric setup and coordinate framework for this flow scenario are depicted in Figure 1.

(1.) Let (u, v, w) be the velocity components along the (x, y, z) directions, respectively.

(2.) A uniform magnetic field of strength B_0 is applied in the z-direction.

(3.) Buoyancy forces are taken in the momentum equations.

(4.) The effects of viscous dissipation and joule heating are not considered in the energy equation.

(5.) In the concentration equation, the chemical reaction effect is neglected.

(6.) Magnetic Reynolds number is assumed very small so that the induced magnetic field is ignored.

(7.) The characteristics of Brownian motion and thermophoresis are accounted for using Buongiorno's model.

(8.) The effect of thermal diffusion (Soret) is considered in the concentration equation and the effect of diffusion thermo (Dufour) is considered in the energy equation.

(9.) The rheological equation for a non-Newtonian fluid is defined as:

$$\tau = \tau_o + \mu\alpha^*. \tag{1}$$

Equation (1) can be expanded for Casson fluid as:

$$\tau_{ij} = \begin{cases} 2\left(\mu_B + \dfrac{p_y}{\sqrt{2\pi}}\right) e_{ij}, & \pi > \pi_c, \\ 2\left(\mu_B + \dfrac{p_y}{\sqrt{2\pi_c}}\right) e_{ij}, & \pi < \pi_c. \end{cases} \tag{2}$$

For this flow, the governing boundary layer equations can be written as:
Continuity equation:

$$\frac{\partial u}{\partial x} + \frac{\partial v}{\partial y} + \frac{\partial w}{\partial z} = 0. \tag{3}$$

Momentum equation:

$$\begin{aligned} &u\left(\frac{\partial u}{\partial x}\right) + v\left(\frac{\partial u}{\partial y}\right) + w\left(\frac{\partial u}{\partial z}\right) \\ &= \nu\left(1 + \frac{1}{\beta}\right)\left(\frac{\partial^2 u}{\partial z^2}\right) - \left(\frac{\sigma B_o^2}{\rho}\right) u \\ &\quad + g\beta_T\left(T - T_\infty\right) + g\beta_C\left(C - C_\infty\right) \\ &\quad + \sqrt{2}\Gamma\left[\frac{\partial u}{\partial z}\right]\left[\frac{\partial^2 u}{\partial z^2}\right], \end{aligned} \tag{4}$$

$$\begin{aligned} &u\left(\frac{\partial v}{\partial x}\right) + v\left(\frac{\partial v}{\partial y}\right) + w\left(\frac{\partial v}{\partial z}\right) \\ &= \nu\left(1 + \frac{1}{\beta}\right)\left(\frac{\partial^2 v}{\partial z^2}\right) - \left(\frac{\sigma B_o^2}{\rho}\right) v \\ &\quad + g\beta_T\left(T - T_\infty\right) + g\beta_C\left(C - C_\infty\right) \\ &\quad + \sqrt{2}\Gamma\left[\frac{\partial v}{\partial z}\right]\left[\frac{\partial^2 v}{\partial z^2}\right]. \end{aligned} \tag{5}$$

Equation of thermal energy:

$$\begin{aligned} &u\left(\frac{\partial T}{\partial x}\right) + v\left(\frac{\partial T}{\partial y}\right) + w\left(\frac{\partial T}{\partial z}\right) \\ &= \alpha\left(\frac{\partial^2 T}{\partial z^2}\right) \\ &\quad + \tau_1\left\{D_B\left(\frac{\partial T}{\partial z}\right)\left(\frac{\partial C}{\partial z}\right) + \frac{D_T}{T_\infty}\left(\frac{\partial T}{\partial z}\right)^2\right\} \\ &\quad + \left(\frac{D_m K_T}{C_S}\right)\left(\frac{\partial^2 C}{\partial z^2}\right). \end{aligned} \tag{6}$$

Equation of species concentration:

$$\begin{aligned} &u\left(\frac{\partial C}{\partial x}\right) + v\left(\frac{\partial C}{\partial y}\right) + w\left(\frac{\partial C}{\partial z}\right) \\ &= D_B\left(\frac{\partial^2 C}{\partial z^2}\right) + \frac{D_T}{T_\infty}\left(\frac{\partial T}{\partial z}\right)^2 \\ &\quad + \left(\frac{D_m K_T}{T_m}\right)\left(\frac{\partial^2 T}{\partial z^2}\right). \end{aligned} \tag{7}$$

Equation of microorganisms:

$$\begin{aligned} &u\left(\frac{\partial \chi}{\partial x}\right) + v\left(\frac{\partial \chi}{\partial y}\right) + w\left(\frac{\partial \chi}{\partial z}\right) \\ &= D_n\left(\frac{\partial^2 \chi}{\partial z^2}\right) - \frac{b^* W_c}{\left(C_w - C_\infty\right)}\frac{\partial}{\partial z}\left(\chi\frac{\partial C}{\partial z}\right). \end{aligned} \tag{8}$$

The boundary conditions for this flow are:

$$\left.\begin{aligned} &u = U_w = U_o \exp\left\{\frac{x+y}{L}\right\}, \\ &v = V_w = V_o \exp\left\{\frac{x+y}{L}\right\}, \\ &-\kappa_f\left(\frac{\partial T}{\partial z}\right) = h_f\left(T_w - T\right), \quad \text{at } z = 0, \\ &-D_B\left(\frac{\partial C}{\partial z}\right) = h_s\left(C_w - C\right), \\ &\chi = \chi_w, \\ &u \to 0,\ v \to 0,\ T \to T_\infty, \\ &C \to C_\infty,\ \chi \to \chi_\infty. \quad \text{as } z \to \infty \end{aligned}\right\} \tag{9}$$

Introducing the following similarity transformations:

$$\left.\begin{aligned} &\eta = \left(\sqrt{\frac{U_o}{2\nu L}}\right)\exp\left[\frac{x+y}{L}\right]z, \\ &u = U_o \exp\left[\frac{x+y}{L}\right] f'\left(\eta\right), \\ &v = V_o \exp\left[\frac{x+y}{L}\right] g'\left(\eta\right),\ \theta = \frac{T - T_\infty}{T_w - T_\infty}, \\ &w = -\left(\sqrt{\frac{\nu U_o}{2L}}\right)\exp\left[\frac{x+y}{L}\right] \\ &\qquad \{f\left(\eta\right) + \eta f'\left(\eta\right) + g\left(\eta\right) + \eta g'\left(\eta\right)\}, \\ &\phi = \frac{C - C_\infty}{C_w - C_\infty},\ N = \frac{\chi - \chi_\infty}{\chi_w - \chi_\infty}. \end{aligned}\right\} \tag{10}$$

Making use of Equation (10), the equation of continuity is identically satisfied and Equations (4)–(8) take the following form:

$$\begin{aligned} &\left(1 + \frac{1}{\beta}\right) f''' + \left(f + g\right) f'' - 2\left(f' + g'\right) f' \\ &\quad + 2\left(\mathrm{Gr}\theta + \mathrm{Gc}\phi\right) - M f' + \lambda f'' f''' = 0, \end{aligned} \tag{11}$$

$$\begin{aligned} &\left(1 + \frac{1}{\beta}\right) g''' + \left(f + g\right) g'' - 2\left(f' + g'\right) g' \\ &\quad + 2\left(\mathrm{Gr}\theta + \mathrm{Gc}\phi\right) - M g' + \lambda g'' g''' = 0, \end{aligned} \tag{12}$$

$$\begin{aligned} &\theta'' + \mathrm{Pr}(f + g)\theta' + \mathrm{PrNb}\theta'\phi' \\ &\quad + \mathrm{PrNt}\theta'^2 + \mathrm{PrDu}\phi'' = 0, \end{aligned} \tag{13}$$

$$\begin{aligned} &\mathrm{Nb}\phi'' + \mathrm{NbLePr}(f + g)\phi' \\ &\quad + \mathrm{Nt}\theta'' + \mathrm{NbSr}\theta'' = 0, \end{aligned} \tag{14}$$

$$\begin{aligned} &N'' + \mathrm{Lb}\left(f + g\right) N' \\ &\quad - \mathrm{Pe}\left(N'\phi' + \phi''\left(N + \Omega\right)\right) = 0, \end{aligned} \tag{15}$$

the corresponding boundary conditions (9) become:

$$\left.\begin{aligned} &f\left(0\right) = 0,\ g\left(0\right) = 0,\ f'\left(0\right) = 1, \\ &g'\left(0\right) = \delta,\ \theta'\left(0\right) = -\delta_1\{1 - \theta\left(0\right)\}, \\ &\phi'\left(0\right) = -\delta_2\{1 - \phi\left(0\right)\},\ N\left(0\right) = 1, \\ &f'\left(\infty\right) \to 0,\ g'\left(\infty\right) \to 0,\ \theta\left(\infty\right) \to 0, \\ &\phi\left(\infty\right) \to 0,\ N\left(\infty\right) \to 0, \end{aligned}\right\} \tag{16}$$

where the involved physical parameters are defined as:

$$\left.\begin{aligned}
&\mathrm{Pr}=\frac{\nu}{\alpha},\ M=\frac{\sigma B_o^2 x}{\rho a},\ \mathrm{Le}=\frac{\nu}{D_B},\\
&\mathrm{Nb}=\frac{(\rho C)_p D_B(C_w-C_\infty)}{(\rho C)_f \nu},\ \lambda=\Gamma x\sqrt{\frac{2a^3}{\nu}},\\
&\delta=\frac{b}{a},\ \mathrm{Sr}=\frac{D_m K_T(T_w-T_\infty)}{T_m\nu\,(C_w-C_\infty)},\\
&\mathrm{Du}=\frac{D_m K_T\,(C_w-C_\infty)}{C_s C_p \nu\,(T-T_\infty)},\\
&\mathrm{Nt}=\frac{(\rho C)_p D_T(T_w-T_\infty)}{(\rho C)_f \nu T_\infty},\ \mathrm{Lb}=\frac{\nu}{D_n},\\
&\mathrm{Pe}=\frac{b^* W_c}{D_n},\ \Omega=\frac{\chi_\infty}{\chi_w-\chi_\infty},\\
&\mathrm{Gr}=\frac{g x^3\beta_T(T_w-T_\infty)}{\nu^2},\\
&\mathrm{Gc}=\frac{g x^3\beta_C(C_w-C_\infty)}{\nu^2}.
\end{aligned}\right\} \quad (17)$$

The physical parameters of the skin-friction coefficient along x and y-directions, local Nusselt number, local Sherwood number, and Motile density coefficients are presented as follows:

$$\begin{aligned}
Cfx &= \left(1+\frac{1}{\beta}\right)\frac{\tau_{wx}}{\rho U_w^2}\\
&= \frac{\mu}{\rho U_w^2}\left(1+\frac{1}{\beta}\right)\left(\frac{\partial u}{\partial z}+\frac{\Gamma}{\sqrt{2}}\left(\frac{\partial u}{\partial z}\right)^2\right)_{z=0} \quad (18)\\
&\Rightarrow \left(\sqrt{Re_x}\right)Cfx\\
&= \left(1+\frac{1}{\beta}\right)\left(1+\frac{\lambda}{2}f''(0)\right)f''(0),
\end{aligned}$$

$$\begin{aligned}
Cfy &= \left(1+\frac{1}{\beta}\right)\frac{\tau_w}{\rho V_w^2}\\
&= \frac{\mu}{\rho V_w^2}\left(1+\frac{1}{\beta}\right)\left(\frac{\partial v}{\partial z}+\frac{\Gamma}{\sqrt{2}}\left(\frac{\partial v}{\partial z}\right)^2\right)_{z=0} \quad (19)\\
&\Rightarrow \left(\sqrt{Re_y}\right)Cfy\\
&= \left(1+\frac{1}{\beta}\right)\left(1+\frac{\lambda}{2}g''(0)\right)g''(0),
\end{aligned}$$

$$\begin{aligned}
\mathrm{Nu} &= \frac{x q_w}{\kappa_f\,(T_w-T_\infty)} = -\frac{x\left(\frac{\partial T}{\partial z}\right)_{z=0}}{\kappa_f\,(T_w-T_\infty)} \quad (20)\\
&\Rightarrow \mathrm{Nu} = -\left(\sqrt{Re_x}\right)\theta'(0),
\end{aligned}$$

$$\begin{aligned}
\mathrm{Sh} &= \frac{x q_m}{D_B\,(C_w-C_\infty)} = -\frac{x\left(\frac{\partial C}{\partial z}\right)_{z=0}}{D_B\,(C_w-C_\infty)} \quad (21)\\
&\Rightarrow \mathrm{Sh} = -\left(\sqrt{Re_x}\right)\phi'(0),
\end{aligned}$$

$$\begin{aligned}
\mathrm{Nh} &= \frac{x d_w}{D_n\,(\chi_w-\chi_\infty)} = -\kappa\left(\frac{\partial \chi}{\partial z}\right)_{z=0} \quad (22)\\
&\Rightarrow \mathrm{Nh} = -\left(\sqrt{Re_x}\right)N'(0).
\end{aligned}$$

3. METHODS

The nonlinear system (11)–(15) with boundary conditions (16) was solved numerically using MATLAB's bvp4c solver, implementing a shooting technique that effectively handles the system's high nonlinearity for accurate approximations.

Step 1: Variable Transformation The higher-order system is converted to a first-order form through the following variable substitutions:

$$\left.\begin{aligned}
&y_1=f,\ y_2=f',\ y_3=f'',\ y_4=g,\\
&y_5=g',\ y_6=g'',\ y_7=\theta,\ y_8=\theta',\\
&y_9=\phi,\ y_{10}=\phi',\ y_{11}=N.
\end{aligned}\right\} \quad (23)$$

Step 2: Reduce the system of higher order nonlinear ODEs in Equations (11)–(15) to a system of first order non-linear ODEs using the new variables in Equation (23):

$$f'''=\frac{-(y_2+y_4)\,y_3+2\,(y_2+y_5)\,y_2 \\ -2\,(Gry_7+\mathrm{Gc}y_9)+My_2}{\left(1+\frac{1}{\beta}\right)+\lambda y_3}, \quad (24)$$

$$g'''=\frac{-(y_1+y_4)\,y_6+2\,(y_2+y_4)\,y_5 \\ -2\,(Gry_7+\mathrm{Gc}y_9)+My_5}{\left(1+\frac{1}{\beta}\right)+\lambda y_6}, \quad (25)$$

$$\begin{aligned}
\theta'' = &-\mathrm{Pr}(y_2+y_4)y_8-\mathrm{PrNb}y_8y_{10}\\
&-\mathrm{PrNt}{y_8}^2-\mathrm{PrDu}\phi'', \quad (26)
\end{aligned}$$

$$\phi''=\frac{-\mathrm{NbLePr}(y_1+y_4)y_{10}-(\mathrm{Nt}+\mathrm{NbSr})\,\theta''}{\mathrm{Nb}}, \quad (27)$$

$$\begin{aligned}
N'' = &-Lby_1y_{12}-Lby_4y_{12}+Pey_{10}y_{12}\\
&+Pey_{11}\phi''+\mathrm{Pe}\Omega\phi''. \quad (28)
\end{aligned}$$

Step 3: Boundary condition transformation The system's boundary conditions from Equation (16) are reformulated using the transformed variables defined in Equation (23):

$$\left.\begin{aligned}
&y_1(0)=0,\ y_4(0)=0,\ y_2(0)=1,\\
&y_4(0)=\delta,\ y_8(0)=-a\{1-y_7(0)\},\\
&y_{10}(0)=-b\{1-y_9(0)\},\ y_{11}(0)=1,\\
&y_2(\infty)\to 0,\ y_5(\infty)\to 0,\ y_7(\infty)\to 0,\\
&y_9(\infty)\to 0,\ y_{11}(\infty)\to 0,
\end{aligned}\right\} \quad (29)$$

where, the subscript notation indicates these evaluation points:

- $\eta=0$ corresponds to the sheet surface,
- $\eta=10$ represents the far-field boundary.

Step 4: In conjunction with the boundary conditions specified in Equation (29), the fourth stage involves using the bvp4c solver to formulate the system of first-order non-linear ordinary differential equations delineated by Equations (24)–(28).

C (δ)	Pr	Rate of heat transfer coefficient results of Vinita Makkar and, Prerna Batra [50]	Current rate of heat transfer coefficient results
0.5	0.7	0.5350077	0.519281587589375
	7.0	2.2614795	2.248287568969821
1.0	0.7	0.6106845	0.620856760578165
	7.0	2.6114286	2.606758295687692

TABLE 1. Results of validation of current rate of heat transfer coefficient with the results of Vinita Makkar and, Prerna Batra [50] when Sr = Du = Lb = Pe = $\Omega = \lambda = 0$.

Step 5: Execute the bvp4c solver sequentially with two separate sets of initial estimates to get the first and second solutions. This assists in identifying primary and secondary responses. The initial estimates will be deemed acceptable if the computed temperature and velocity profiles conform to Equation (16); if not, this procedure will be repeated with a new set of initial assumptions until the desired outcomes are achieved. Typically, several attempts are required to get a satisfactory compilation of first observations.

4. Program code validation

In absence of Thermal diffusion (Soret), Diffusion thermo (Dufour), Bioconvection Lewis number, Peclet number, Microorganism difference parameter, and Williamson fluid parameter, the authors have compared present numerical results of the heat transfer rate coefficient with the published results of Vinita Makkar and, Prerna Batra [50] for variations of $C(\delta)$ and Pr in Table 1. It shows a good agreement between the current findings and those obtained by Vinita Makkar and, Prerna Batra [50], as previously stated.

Here C – stretching sheet ratio parameter of Vinita Makkar and, Prerna Batra [50] & δ – stretching sheet ratio parameter of this study.

5. Results and discussion

The present investigation explores the complex interplay of multiple physical phenomena in a three-dimensional MHD Williamson-Casson nanofluid flow over an exponentially stretching sheet. The coupled effects of thermal diffusion (Soret), diffusion thermo (Dufour), buoyancy forces, and gyrotactic microorganisms are analysed through numerical solutions obtained using MATLAB's bvp4c solver. The key findings are systematically presented below.

5.1. Flow characteristics and velocity profiles

Magnetic (M): Figures 2–3 demonstrate that increasing the magnetic parameter ($M = 0.1$ to 0.7) significantly reduces both primary ($f'(\eta)$) and secondary ($g'(\eta)$) velocity profiles. This retardation effect stems from the Lorentz force, which creates a resistive drag perpendicular to both the fluid motion and the applied magnetic field.

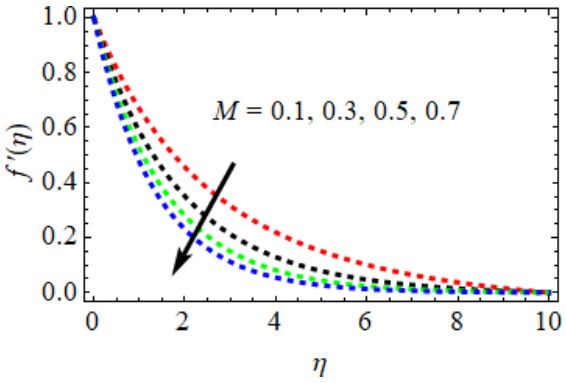

FIGURE 2. Effect of M on $f'(\eta)$.

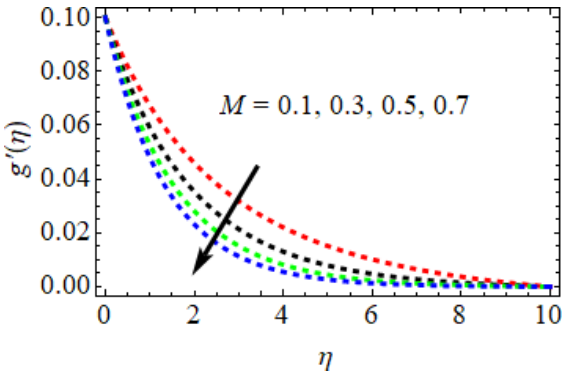

FIGURE 3. Effect of M on $g'(\eta)$.

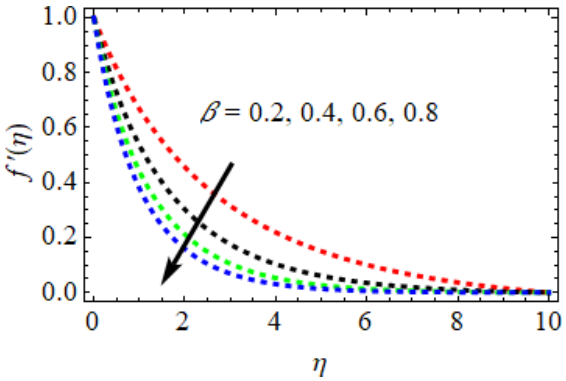

FIGURE 4. Effect of β on $f'(\eta)$.

Non-Newtonian fluid behaviour: The Casson parameter (β) exhibits a dual role (Figures 4–5). While higher β values (0.2 to 0.8) enhance yield stress, they simultaneously stabilise the flow by reducing deformation rates.

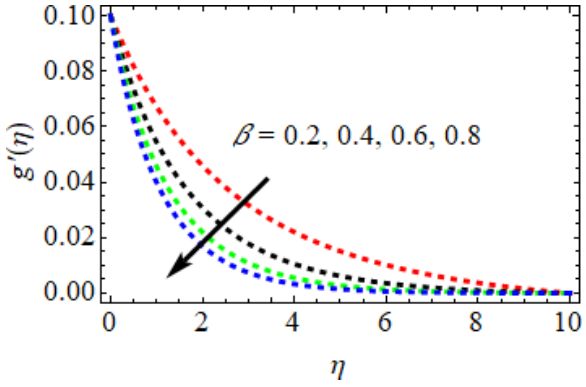

Figure 5. Effect of β on $g'(\eta)$.

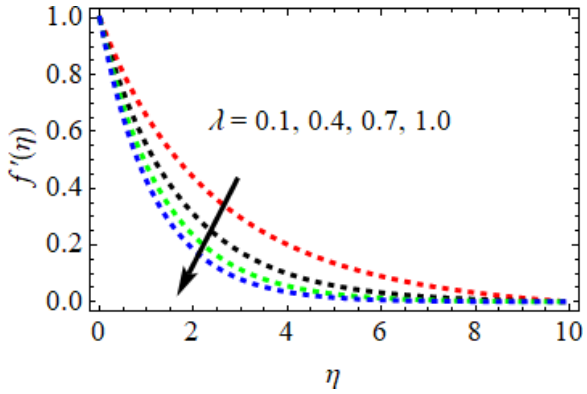

Figure 6. Effect of λ on $f'(\eta)$.

The Williamson parameter (λ) shows shear-thinning characteristics (Figures 6–7), where increasing λ (0.1 to 1.0) decreases velocities due to enhanced apparent viscosity at higher shear rates.

Buoyancy-driven effects: Thermal (Gr) and solutal (Gc) Grashof numbers exhibit similar trends (Figures 8–11). As Gr increases from 0.5 to 1.5, the velocity boundary layer thickens due to stronger thermal buoyancy. Analogously, Gc (0.5 to 1.2) enhances momentum transport through concentration-induced buoyancy.

Stretching dynamics: Figure 12 reveals that the stretching ratio parameter ($\delta = 0.5$ to 2.0) amplifies secondary velocities by modifying the surface kinematics.

5.2. Thermal transport mechanisms

Prandtl number (Pr): Figure 13 highlights the inverse relationship between Pr (0.71 to 7.0) and the thermal boundary layer thickness. Higher Pr fluids (e.g. water at Pr $\approx$ 7) exhibit steeper temperature gradients due to reduced thermal diffusivity.

Nanoparticle effects: Brownian motion (Nb) and thermophoresis (Nt) parameters significantly alter heat transfer (Figures 14–17). Nb (0.3 to 0.7) enhances thermal conductivity through random nanoparticle motion, while Nt (0.2 to 1.0) drives particle migration along temperature gradients.

Cross-diffusion phenomena: The Dufour effect (Du = 0.5 to 1.5, Figure 18) increases temperatures by converting concentration gradients into thermal energy. Conversely, the Soret effect (Sr = 0.5 to 1.5, Figure 19) augments mass transfer via thermally induced diffusion.

5.3. Mass transfer and microorganism distributions

Lewis number (Le): Figure 20 shows that increasing Le (0.5 to 1.5) thins the concentration boundary layer, as higher Le results in slower mass diffusion relative to thermal diffusion.

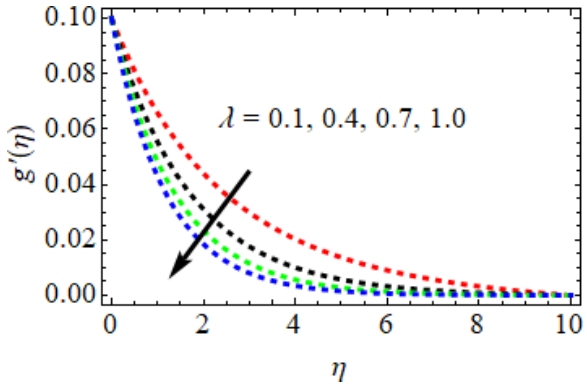

Figure 7. Effect of λ on $g'(\eta)$.

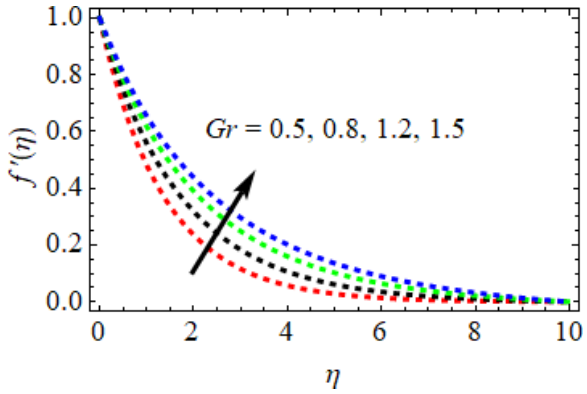

Figure 8. Effect of Gr on $f'(\eta)$.

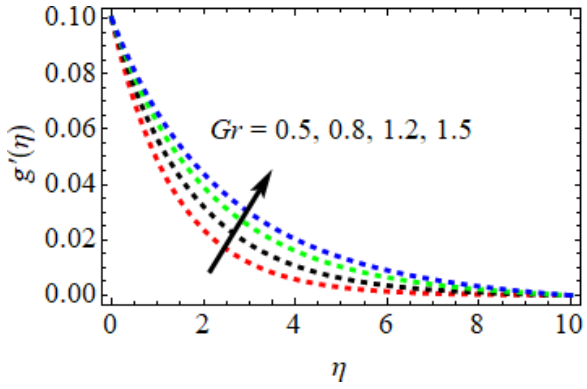

Figure 9. Effect of Gr on $g'(\eta)$.

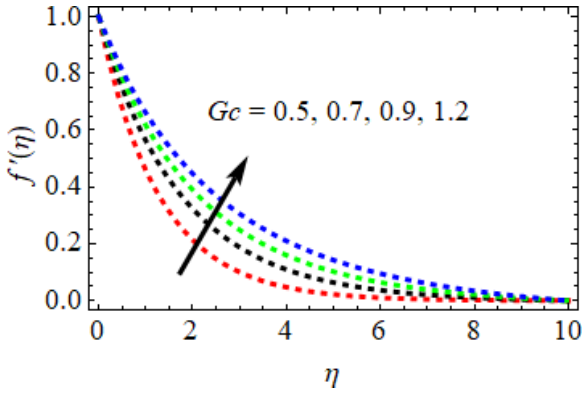

FIGURE 10. Effect of Gc on $f'(\eta)$.

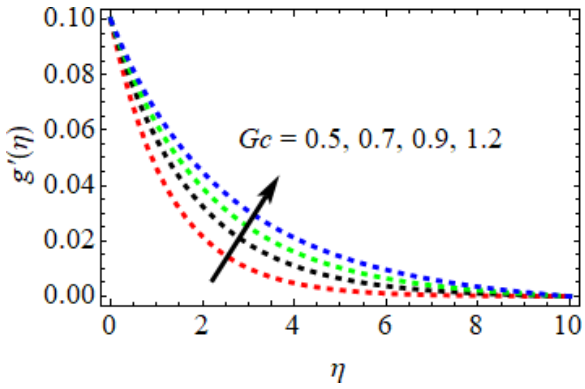

FIGURE 11. Effect of Gc on $g'(\eta)$.

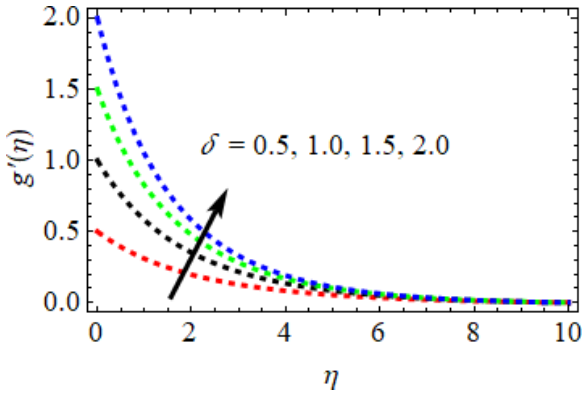

FIGURE 12. Effect of δ on $g'(\eta)$.

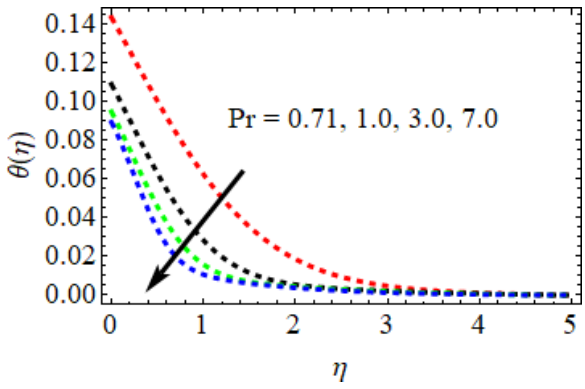

FIGURE 13. Effect of Pr on $\theta(\eta)$.

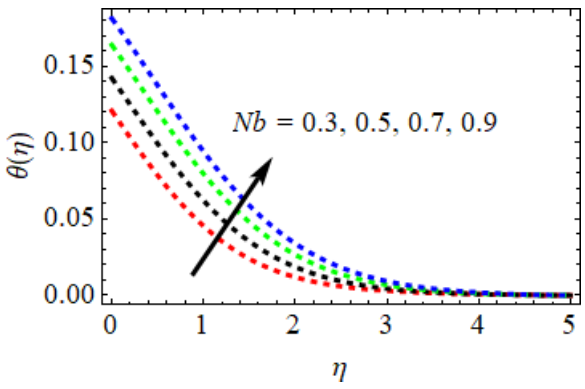

FIGURE 14. Effect of Nb on $\theta(\eta)$.

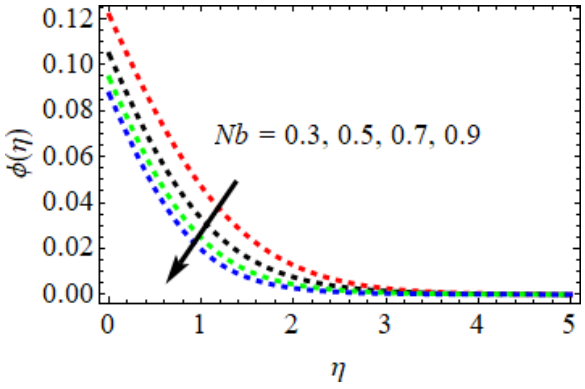

FIGURE 15. Effect of Nb on $\phi(\eta)$.

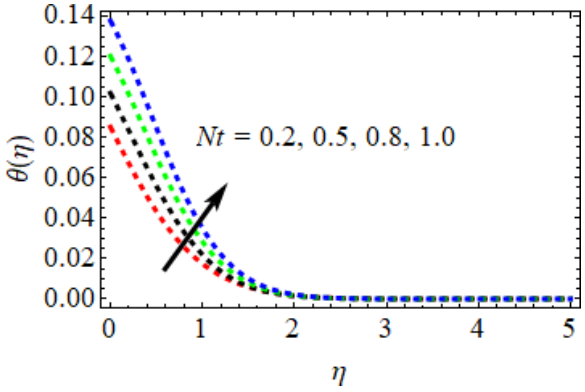

FIGURE 16. Effect of Nt on $\theta(\eta)$.

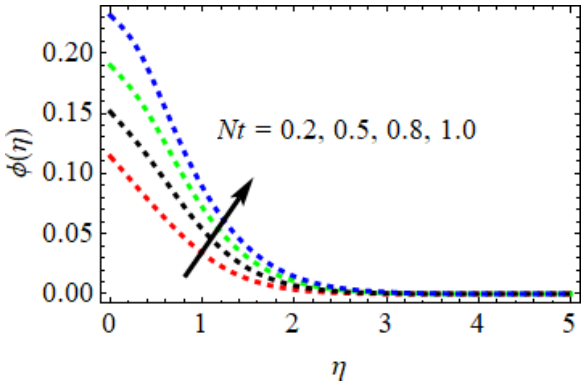

FIGURE 17. Effect of Nt on $\phi(\eta)$.

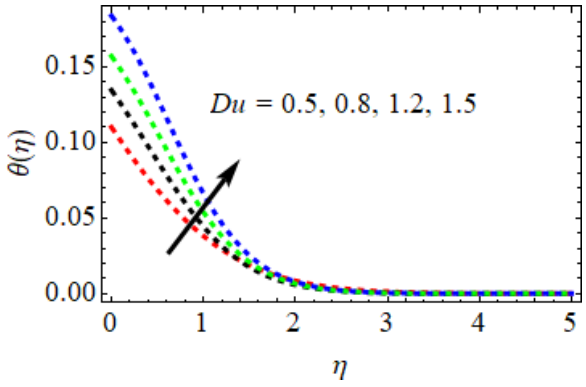

Figure 18. Effect of Du on $\theta(\eta)$.

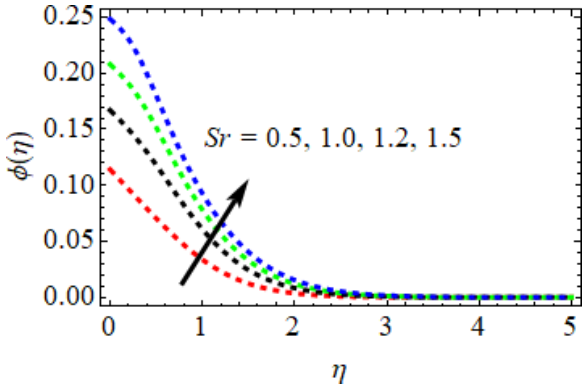

Figure 19. Effect of Sr on $\phi(\eta)$.

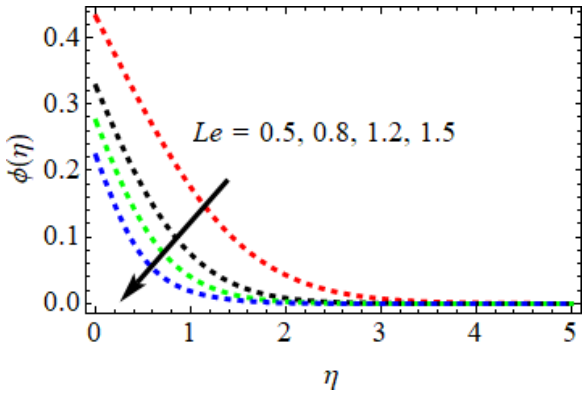

Figure 20. Effect of Le on $\phi(\eta)$.

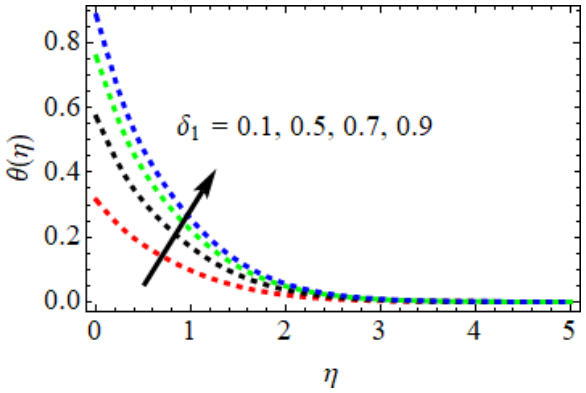

Figure 21. Effect of δ_1 on $\theta(\eta)$.

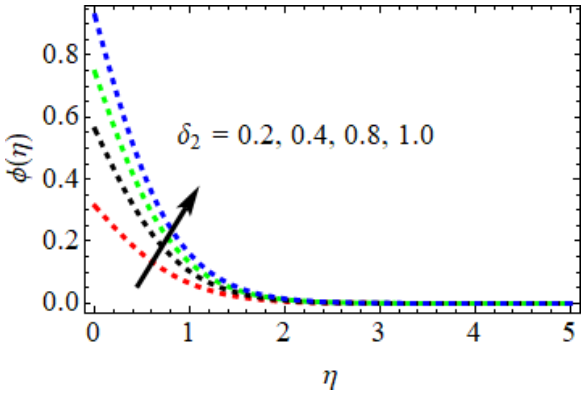

Figure 22. Effect of δ_2 on $\phi(\eta)$.

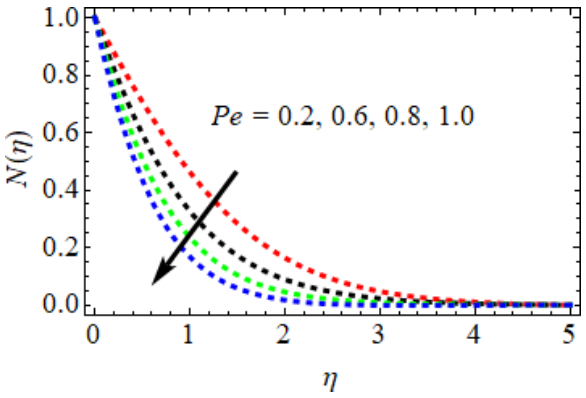

Figure 23. Effect of Pe on $N(\eta)$.

Biot numbers: Thermal (δ_1) and mass (δ_2) Biot numbers govern the convective boundary conditions. Figures 21–22 illustrate that δ_1 (0.1 to 0.91) and δ_2 (0.2 to 1.0) increase the temperature and concentration gradients near the sheet surface, respectively.

Bioconvection parameters: The Peclet number (Pe = 0.2 to 0.8, Figure 23) and bioconvection Lewis number (Lb = 0.3 to 0.9, Figure 24) reduce the microorganism density ($N(\eta)$) by promoting convective transport over diffusive spreading. Figure 25 shows that a higher microorganism concentration gradient reduces motile bacteria density and alters their boundary layer.

5.4. Engineering quantities of interest

Skin-friction coefficients: Tables 2–5 quantify how Cfx and Cfy vary with parameters. For instance, Cfx increases by 8.2 % when Gr rises from 0.5 to 1.5, but decreases by 6.5 % for $M = 0.1$ to 0.7.

Nusselt and Sherwood numbers: Table 6 shows that Nu increases by 12.3 % for Nb = 0.3 to 0.7, but decreases by 9.2 % for Pr = 0.71 to 7.0. Table 7 indicates that Sh increases by 14.7 % for Nt = 0.2 to 0.8, but decreases by 8.1 % for Le = 0.5 to 1.2.

Motile density coefficient: Table 8 reveals that Nh decreases by 15.4 % as Lb increases from 0.3 to 0.9.

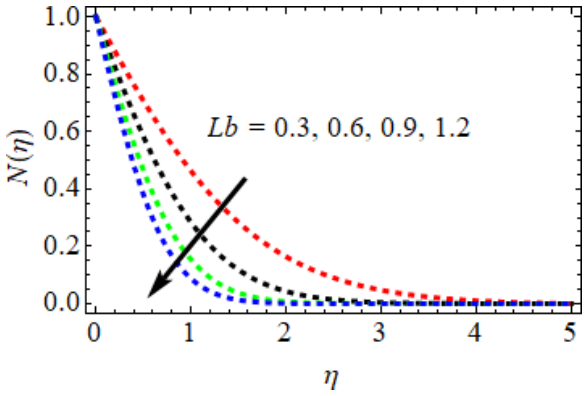

FIGURE 24. Effect of Lb on $N(\eta)$.

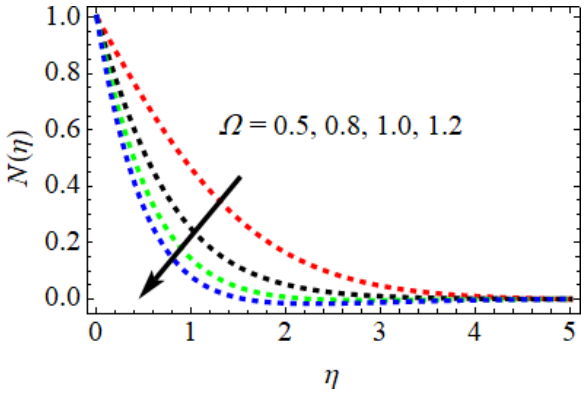

FIGURE 25. Effect of Ω on $N(\eta)$.

M	β	λ	Gr	Gc	δ	Pr	Nb	Nt	$\left(1+\frac{1}{\beta}\right)\left(1+\frac{\lambda}{2}f''(0)\right)f''(0)$
0.1	0.2	0.1	0.5	0.5	0.5	0.71	0.3	0.2	3.4657648158
0.3									3.4289756871
0.5									3.4026578915
	0.4								3.4256756103
	0.6								3.3967304625
		0.4							3.4312875687
		0.7							3.4078760936
			0.8						3.4934809851
			1.2						3.5106587215
				0.7					3.5089763091
				0.9					3.5376803164
					1.0				3.5188582768
					1.5				3.5497567831
						1.00			3.4163546593
						7.00			3.3867645811
							0.5		3.4867630746
							0.7		3.5078640652
								0.5	3.4976290333
								0.8	3.5146903609

TABLE 2. Computational values of Skin-friction coefficient $\left(1+\frac{1}{\beta}\right)\left(1+\frac{\lambda}{2}f''(0)\right)f''(0)$.

M	β	λ	Gr	Gc	δ	Pr	Nb	Nt	$\left(1+\frac{1}{\beta}\right)\left(1+\frac{\lambda}{2}g''(0)\right)g''(0)$
0.1	0.2	0.1	0.5	0.5	0.5	0.71	0.3	0.2	2.8276029639
0.3									2.7958618501
0.5									2.7650651906
	0.4								2.8009609561
	0.6								2.7814774574
		0.4							2.7956708156
		0.7							2.7730460521
			0.8						2.8560146066
			1.2						2.8845025807
				0.7					2.8665016055
				0.9					2.9016082752
					1.0				2.8538765701
					1.5				2.8740657611
						1.00			2.7856861802
						7.00			2.7507647601
							0.5		2.8465876019
							0.7		2.8607620862
								0.5	2.8500569615
								0.8	2.8701695900

TABLE 3. Computational values of Skin-friction coefficient $\left(1+\frac{1}{\beta}\right)\left(1+\frac{\lambda}{2}g''(0)\right)g''(0)$.

Du	**Sr**	**Le**	$\boldsymbol{\delta_1}$	$\boldsymbol{\delta_2}$	**Lb**	**Pe**	**Ω**	$\left(1+\frac{1}{\beta}\right)\left(1+\frac{\lambda}{2}f''(0)\right)f''(0)$
0.5	0.5	0.5	0.1	0.2	0.3	0.2	0.5	3.4657648158
0.8								3.4860591649
1.2								3.5014675245
	1.0							3.4967919099
	1.2							3.5168576821
		0.8						3.4389787653
		1.2						3.4067601645
			0.5					3.4967976903
			0.7					3.5132548344
				0.4				3.4906636091
				0.8				3.5298782815
					0.6			3.4296857681
					0.9			3.4016874432
						0.6		3.4160165091
						0.8		3.3901650926
							0.8	3.4086617871
							1.0	3.3815626506

Table 4. Computational values of Skin-friction coefficient $\left(1+\frac{1}{\beta}\right)\left(1+\frac{\lambda}{2}f''(0)\right)f''(0)$.

Du	**Sr**	**Le**	$\boldsymbol{\delta_1}$	$\boldsymbol{\delta_2}$	**Lb**	**Pe**	**Ω**	$\left(1+\frac{1}{\beta}\right)\left(1+\frac{\lambda}{2}g''(0)\right)g''(0)$
0.5	0.5	0.5	0.1	0.2	0.3	0.2	0.5	2.8276029639
0.8								2.8506501650
1.2								2.8746545944
	1.0							2.8466791091
	1.2							2.8604665026
		0.8						2.7930762507
		1.2						2.7714872563
			0.5					2.8560691691
			0.7					2.8719676362
				0.4				2.8406065019
				0.8				2.8673065072
					0.6			2.7856064675
					0.9			2.7606756101
						0.6		2.7906967013
						0.8		2.7706767517
							0.8	2.7807657251
							1.0	2.7610607682

Table 5. Computational values of Skin-friction coefficient $\left(1+\frac{1}{\beta}\right)\left(1+\frac{\lambda}{2}g''(0)\right)g''(0)$.

Pr	**Nb**	**Nt**	**Du**	$\boldsymbol{\delta_1}$	**Nu**
0.71	0.3	0.2	0.5	0.1	1.5606056108
1.00					1.5395786181
7.00					1.5038959821
	0.5				1.5809881953
	0.7				1.6084650711
		0.5			1.5969019193
		0.8			1.6154865298
			0.8		1.6056704184
			1.2		1.6248568223
				0.5	1.5986797903
				0.7	1.6145474856

Table 6. Computational values of heat transfer rate coefficient for variations of Pr, Nb, Nt, Du, and δ_1.

Le	**Nb**	**Nt**	**Sr**	$\boldsymbol{\delta_2}$	**Sh**
0.5	0.3	0.2	0.5	0.2	2.2657657870
0.8					2.2485465567
1.2					2.2087635568
	0.5				2.2307657812
	0.7				2.2067806146
		0.5			2.2967604176
		0.8			2.3156589552
			1.0		2.3067160464
			1.2		2.3265876851
				0.4	2.2856708725
				0.8	2.3057787447

Table 7. Computational values of mass transfer rate coefficient for variations of Le, Nb, Nt, Sr, and δ_2.

Lb	Pe	Ω	Nh
0.3	0.2	0.5	1.3856847618
0.6			1.3506576101
0.9			1.3396760936
	0.6		1.3587636401
	0.8		1.3306763109
		0.8	1.3490619364
		1.0	1.3076870139

TABLE 8. Computational values of motile density coefficient for variations of Lb, Pe, and Ω.

5.5. VALIDATION AND COMPARATIVE ANALYSIS

Table 1 validates the numerical methodology by comparing heat transfer rates (Nu) with previous study [50]. The maximum deviation of 2.9 % confirms the solution accuracy.

6. CONCLUSION

The objective of this study was to examine the physics of fluid flow, particularly the interconnected diffusion effects of Williamson-Casson fluid flowing over a stretched sheet in the presence of microorganisms, nanoparticles, buoyancy forces, temperature Biot number, mass Biot number, and magnetic fields. To show how the engineering factors affect the primary velocity, secondary velocity, temperature, concentration, and microorganism profiles, we used the appropriate mathematical approaches to modify the differential equations that describe the phenomena. Graphs were then used to show what happened after this modification. The following is a complete list of the most important findings:

- To improve the primary and secondary velocity profiles, the Casson parameter must be increased. This is because fluids with minimal shear stress do not yield easily. On the other hand, raising the shear stresses will cause yielding, which will make the flow more stable and faster.
- The thermal and mass Grashof numbers both help to improve the primary and secondary velocity profiles. This shows how buoyancy forces are affected by changes in temperature and concentration gradients.
- The research revealed that the magnetic parameter adversely affected both the primary and secondary velocity profiles.
- The Prandtl number decreased the temperature profiles, while the Dufour number, thermophoresis, and Brownian motion effects increased them.
- The temperature profiles increase as the thermal Biot number increases.
- The Soret number, mass Biot number, and thermophoresis show better concentration profiles. Conversely, the increase in the Lewis number and Brownian motion has led to a decrease in these concentration patterns.

In conclusion, given the limited values of these parameters, a comparison between the present research and the work of Vinita Makkar and Prerna Batra [50] is warranted.

Limitations: it neglects viscous dissipation and Joule heating, which may affect thermal behaviour in high-velocity or high-magnetic-field flows. Chemical reactions and induced magnetic fields are ignored, restricting applicability. Numerical solutions rely on approximations, and far-field boundary conditions may not fully capture asymptotic behaviour. Experimental validation is lacking, limiting real-world reliability. Microorganism dynamics are simplified, assuming uniform behaviour without considering spatial heterogeneity or adaptive responses. These constraints suggest the need for more comprehensive modelling and empirical verification.

Future research directions

- Enhance models with viscous dissipation, Joule heating, and chemical reactions.
- Use advanced numerical methods such as machine learning for complex nonlinearities.
- Validate findings experimentally, especially for bioconvection.
- Study microorganism-nanoparticle interactions and industrial applications.
- Explore flows over complex geometries (e.g. wavy walls) for real-world relevance.
- Optimise parameters for cooling and biomedical applications.

LIST OF SYMBOLS

u, v, w Velocity components in x, y and z axes respectively $[\mathrm{m\,s^{-1}}]$

x, y, z Cartesian coordinates measured along the stretching sheet [m]

f Dimensionless stream function along x-direction $[\mathrm{kg\,(m\,s)^{-1}}]$

f' Fluid velocity along x-direction $[\mathrm{m\,s^{-1}}]$

q_w Heat flux coefficient

g Dimensionless stream function along y-direction $[\mathrm{kg\,m^{-1}\,s^{-1}}]$

g' Fluid velocity along y-direction $[\mathrm{m\,s^{-1}}]$

Pr Prandtl number

T Fluid temperature [K]

T_w Temperature at the surface [K]

B_o Uniform magnetic field [Tesla]

M Magnetic field parameter

T_∞ Temperature of the fluid far away from the stretching sheet [K]

Cfx Skin-friction coefficient along x-direction $[\mathrm{s^{-1}}]$

V_o Reference velocity $[\mathrm{m\,s^{-1}}]$

Cfy Skin-friction coefficient along y-direction $[\mathrm{s}^{-1}]$
$U_w(x)$ Stretching velocity of the fluid along x-direction $[\mathrm{m\,s}^{-1}]$
$V_w(y)$ Stretching velocity of the fluid along y-direction $[\mathrm{m\,s}^{-1}]$
q_m Mass flux coefficient
Le Lewis number
Nt Thermophoresis parameter
Nb Brownian motion parameter
Sr Soret number
Du Dufour number
Nu Rate of heat transfer coefficient (or) Nusselt number
Sh Rate of mass transfer coefficient (or) Sherwood number
C_p Specific heat capacity of nano particles $[\mathrm{J\,kg}^{-1}\,\mathrm{K}^{-1}]$
a, b Constants
Re_x Reynolds number along x-direction
Re_y Reynolds number along y-direction
D_B Brownian diffusion coefficient $[\mathrm{m}^2\,\mathrm{s}^{-1}]$
D_T Thermophoresis diffusion coefficient
C Dimensional Fluid concentration $[\mathrm{mol\,m}^{-3}]$
C_w Dimensional concentration at the stretching surface $[\mathrm{mol\,m}^{-3}]$
W_c Cell swimming speed
C_∞ Dimensional ambient volume fraction $[\mathrm{mol\,m}^{-3}]$
g Acceleration due to gravity $[\mathrm{m\,s}^{-2}]$
U_o Reference velocity $[\mathrm{m\,s}^{-1}]$
L Length of Reference
D_n Solutal diffusivity of the medium
b^* Chemotaxis constant
Nh Motile density
N Dimensionless microorganism profiles
Le Bioconvection Lewis number
Pe Peclet number
T_m Mean fluid temperature
p_y Yield stress of the fluid
C_s Concentration susceptibility
K_T Thermal diffusion ratio
D_m Mass diffusion
Gr Grashof number for heat transfer
Gc Grashof number for mass transfer
h_f Coefficient of convective heat transfer
h_s Coefficient of convective mass transfer
π Deformation rate
π_c Critical value of non-Newtonian model
α Thermal diffusivity $[\mathrm{m}^2\,\mathrm{s}^{-1}]$
β_T Thermal coefficient expansion
β_C Concentration coefficient

Greek symbols

Ω Microorganism difference parameter
χ Dimensional Microorganism profiles
χ_w Microorganism at the surface
χ_∞ Ambient microorganism
λ Williamson fluid parameter
η Dimensionless similarity variable [m]
θ Dimensionless temperature [K]
ν Kinematic viscosity $[\mathrm{m}^2\,\mathrm{s}^{-1}]$
σ Electrical conductivity
ρ Fluid density $[\mathrm{kg\,m}^{-3}]$
μ Dynamic viscosity of the fluid
κ_f Thermal conductivity of the fluid
α^* Shear rate
β Casson fluid parameter
μ_B Dynamic viscosity of the Casson fluid
τ Cauchy stress tensor
τ_{wx} Wall shear stress along x-direction
τ_{wy} Wall shear stress along y-direction
ϕ Dimensionless nano-fluid concentration $[\mathrm{mol\,m}^{-3}]$
τ_1 Parameter defined as $\frac{(\rho C)_p}{(\rho C)_f}$
δ Stretching sheet parameter

Superscript

$'$ Differentiation w.r.t η

Subscripts

f Fluid
w Condition on the sheet
∞ Ambient conditions

References

[1] S. Reddy, P. B. A. Reddy, A. J. Chamkha. MHD flow analysis with water-based CNT nanofluid over a non-linear inclined stretching/shrinking sheet considering heat generation. *Chemical Engineering Transactions* **71**:1003–1008, 2018. https://doi.org/10.3303/CET1871168

[2] A. Hussanan, I. Khan, M. R. Gorji, W. A. Khan. $\mathrm{CNT_S}$ – water-based nanofluid over a stretching sheet. *BioNanoScience* **9**(1):21–29, 2019. https://doi.org/10.1007/s12668-018-0592-6

[3] B. Mahanthesh, B. J. Gireesha, I. L. Animasaun, et al. MHD flow of SWCNT and MWCNT nanoliquids past a rotating stretchable disk with thermal and exponential space dependent heat source. *Physica Scripta* **94**(8):085214, 2019. https://doi.org/10.1088/1402-4896/ab18ba

[4] A. Tulu, W. Ibrahim. MHD slip flow of CNT-ethylene glycol nanofluid due to a stretchable rotating disk with Cattaneo-Christov heat flux model. *Mathematical Problems in Engineering* **2020**(1):1374658, 2020. https://doi.org/10.1155/2020/1374658

[5] K. Muhammad, T. Hayat, Alsaedi. OHAM analysis of Newtonian heating in mixed convective flow of CNTs over a stretched cylinder. *Alexandria Engineering Journal* **61**(5):3697–3707, 2022. https://doi.org/10.1016/j.aej.2021.08.072

[6] F. Shah, T. Hayat, A. Alsaedi. Entropy optimization in a fourth grade nanofluid flow over a stretchable Riga wall with thermal radiation and viscous dissipation. *International Communications in Heat and Mass Transfer* **127**:105398, 2021. https://doi.org/10.1016/j.icheatmasstransfer.2021.105398

[7] A. Salamah Aljaloud, L. Manai, I. Tlili. Flow of couple stress nanofluid due to stretching surface with applications of induced magnetic field and variable thermal conductivity. *Case Studies in Thermal*

Engineering **57**:104356, 2024.
https://doi.org/10.1016/j.csite.2024.104356

[8] M. Amjad, I. Zehra, S. Nadeem, et al. Influence of Lorentz force and induced magnetic field effects on Casson Micropolar nanofluid flow over a permeable curved stretching/shrinking surface under the stagnation region. *Surfaces and Interfaces* **21**:100766, 2020.
https://doi.org/10.1016/j.surfin.2020.100766

[9] M. I. Khan, F. Alzahrani. Nonlinear dissipative slip flow of Jeffrey nanomaterial towards a curved surface with entropy generation and activation energy. *Mathematics and Computers in Simulation* **185**:47–61, 2021.
https://doi.org/10.1016/j.matcom.2020.12.004

[10] F. Shah, M. I. Khan, Y.-M. Chu, S. Kadry. Heat transfer analysis on MHD flow over a stretchable Riga wall considering entropy generation rate: A numerical study. *Numerical Methods for Partial Differential Equations* **40**(1):e22694, 2024.
https://doi.org/10.1002/num.22694

[11] M. N. Othman, A. Jedi, N. A. A. Bakar. MHD stagnation point on nanofluid flow and heat transfer of carbon nanotube over a shrinking surface with heat sink effect. *Molecules* **26**(24):7441, 2021.
https://doi.org/10.3390/molecules26247441

[12] A. Majeed, A. Zeeshan, T. Alam. Mathematical analysis of MHD CNT's of rotating nanofluid flow over a permeable stretching surface. *Arabian Journal for Science and Engineering* **48**(1):727–737, 2023.
https://doi.org/10.1007/s13369-022-06871-w

[13] N. A. A. Samat, N. Bachok, N. M. Arifin. Carbon nanotubes (CNTs) nanofluids flow and heat transfer under MHD effect over a moving surface. *Journal of Advanced Research in Fluid Mechanics and Thermal Sciences* **103**(1):165–178, 2023.
https://doi.org/10.37934/arfmts.103.1.165178

[14] N. Vishnu Ganesh, A. K. Abdul Hakeem, B. Ganga. Darcy–Forchheimer flow of hydromagnetic nanofluid over a stretching/shrinking sheet in a thermally stratified porous medium with second order slip, viscous and ohmic dissipations effects. *Ain Shams Engineering Journal* **9**(4):939–951, 2018.
https://doi.org/10.1016/j.asej.2016.04.019

[15] M. Jawad, M. K. Hameed, K. S. Nisar, A. H. Majeed. Darcy-Forchheimer flow of Maxwell nanofluid flow over a porous stretching sheet with Arrhenius activation energy and Nield boundary conditions. *Case Studies in Thermal Engineering* **44**:102830, 2023.
https://doi.org/10.1016/j.csite.2023.102830

[16] P. Agarwal, R. Jain, K. Loganathan. Thermally radiative flow of MHD Powell-Eyring nanofluid over an exponential stretching sheet with swimming microorganisms and viscous dissipation: A numerical computation. *International Journal of Thermofluids* **23**:100773, 2024.
https://doi.org/10.1016/j.ijft.2024.100773

[17] P. Choudhary, S. Choudhary, K. Jat, et al. Impacts of unsteady MHD hybrid nanofluid over a non-linear stretchable porous sheet with thermal radiation and gyrotatic microorganisms. *International Journal of Thermofluids* **23**:100788, 2024.
https://doi.org/10.1016/j.ijft.2024.100788

[18] P. Rana, M. Basavarajappa. Bioconvection dynamics in rotating and stationary cone-disk systems. *Physics of Fluids* **36**(11):112038, 2024.
https://doi.org/10.1063/5.0239637

[19] M. R. Moradi, K. Hosseinzadeh, A. Hasibi, D. D. Ganji. Hydrothermal study on nano-bioconvective fluid flow over a vertical plate under the effect of magnetic field. *Numerical Heat Transfer, Part B: Fundamentals* **85**(4):469–483, 2024.
https://doi.org/10.1080/10407790.2023.2241632

[20] E. A. Algehyne, F. M. Alamrani, S. A. Lone, et al. Numerical exploration of radiative heat transfers in a magneto bioconvection Maxwell fluid passing through a spinning disk. *Advances in Mechanical Engineering* **16**(10):16878132241282017, 2024.
https://doi.org/10.1177/16878132241282017

[21] M. R. Khan, V. Puneeth, M. K. Alaoui, A. O. Almagrabi. Numerical simulation of unsteady MHD bio-convective flow of viscous nanofluid through a stretching surface. *Case Studies in Thermal Engineering* **53**:103830, 2024.
https://doi.org/10.1016/j.csite.2023.103830

[22] Y. Wu, M. Chaudhry, N. Maqbool, et al. Entropy generation in radiative motion of tangent hyperbolic nanofluid in the presence of gyrotactic microorganisms and activation energy. *Frontiers in Physics* **12**:1409318, 2024. https://doi.org/10.3389/fphy.2024.1409318

[23] M. Chaudhry, M. A. Basit, M. Imran, et al. Numerical analysis of mathematical model of nanofluid flow through stagnation point involving thermal radiation, activation energy, and living organisms. *AIP Advances* **15**(1):015220, 2025.
https://doi.org/10.1063/5.0249122

[24] S. R. Mishra, T. M. Agbaje, R. Baithalu, S. Panda. Spectral quasi-linearization approach for the swimming of motile microorganisms on the bio-convection Casson nanofluid flow over a rotating circular disk. *Numerical Heat Transfer, Part B: Fundamentals* **86**(9):3039–3065, 2025.
https://doi.org/10.1080/10407790.2024.2352857

[25] Y. Aboel-Magd, A. Basem, U. Farooq, et al. Computational modeling of thermal radiation and activation energy effects in Casson nanofluid flow with bioconvection and microorganisms over a disk. *International Journal of Thermofluids* **23**:100735, 2024.
https://doi.org/10.1016/j.ijft.2024.100735

[26] N. S. Khan, U. W. Humphries, W. Kumam, et al. Bioconvection Casson nanoliquid film sprayed on a stretching cylinder in the portfolio of homogeneous-heterogeneous chemical reactions. *ZAMM – Journal of Applied Mathematics and Mechanics* **102**(5):e202000222, 2022. https://doi.org/10.1002/zamm.202000222

[27] N. S. Khan, S. Sriyab, A. Kaewkhao, E. Thawinan. Hall current effect in bioconvection Oldroyd-B nanofluid flow through a porous medium with Cattaneo-Christov heat and mass flux theory. *Scientific Reports* **12**(1):19821, 2022. https://doi.org/10.1038/s41598-022-23932-0

[28] A. M. Rashad, H. A. Nabwey. Gyrotactic mixed bioconvection flow of a nanofluid past a circular cylinder with convective boundary condition. *Journal of the Taiwan Institute of Chemical Engineers* **99**:9–17, 2019.
https://doi.org/10.1016/j.jtice.2019.02.035

[29] M. Ferdows, K. Zaimi, A. M. Rashad, H. A. Nabwey. MHD bioconvection flow and heat transfer of nanofluid through an exponentially stretchable sheet. *Symmetry* **12**(5):692, 2020. https://doi.org/10.3390/sym12050692

[30] H. A. Nabwey, S. I. Alshber, A. M. Rashad, A. E. N. Mahdy. Influence of bioconvection and chemical reaction on Magneto-Carreau nanofluid flow through an inclined cylinder. *Mathematics* **10**(3):504, 2022. https://doi.org/10.3390/math10030504

[31] D. R. Kirubaharan, A. D. Subhashini, M. Gundagani. Study of three dimensional Casson-nanofluid flow due to a linear porous stretching sheet in the presence of double diffusion effects. *Advances in Systems Science and Applications* **24**(3):90–103, 2024. https://doi.org/10.25728/assa.2024.2024.03.1539

[32] M. Gundagani, G. Deepa, J. V. Madhu, et al. Three dimensional chemically reacting Oldroyd-B fluid + nanofluid flow in presence of thermophoresis and Brownian motion effects. *Discontinuity, Nonlinearity, and Complexity* **14**(2):373–388, 2025. https://doi.org/10.5890/DNC.2025.06.010

[33] P. K. Tanuku, L. P. Mamidi, M. Gundagani. Modelling and analysis of three-dimensional chemically reacting, radiating Casson-nanofluid flow: Thermophoresis and Brownian motion effects. *Acta Polytechnica* **64**(5):455–463, 2024. https://doi.org/10.14311/AP.2024.64.0455

[34] M. Gundagani, P. Lakshmi, M. Amarnath, et al. Three-dimensional MHD flow of a radiative Eyring-Powell nanofluid: Exploring Hall effects and heat transfer. *Theoretical and Mathematical Physics* **223**(3):1070–1086, 2025. https://doi.org/10.1134/S0040577925060170

[35] M. Gundagani, J. Venkata Madhu, G. Deepa, et al. Hall current and MHD impacts on a 3D Maxwell nanofluid flow across a porous stretching surface. *Theoretical and Mathematical Physics* **223**(3):899–914, 2025. https://doi.org/10.1134/S0040577925060030

[36] P. Tanuku, L. Mamidi, M. Gundagani. Modelling and analysis of three-dimensional Maxwell-nanofluid flow over a bi-directional stretching surface in the presence of a magnetic field. *International Journal for Engineering Modelling* **38**(1):53–72, 2025. https://doi.org/10.31534/engmod.2025.1.ri.04d

[37] S. Sheri, M. Gundagani, M. P. Karanamu. Analysis of heat and mass transfer effects on an isothermal vertical oscillating plate. *Walailak Journal of Science and Technology (WJST)* **9**(4):407–415, 2012.

[38] M. Gundagani, J. Venkata Madhu, G. Deepa, et al. Three-dimensional Oldroyd-B fluid flow past a stretching surface with magnetic field, nanofluid particles and Cattaneo-Christov double diffusion effects. *Johnson Matthey Technology Review* **69**(2):299–320, 2025. https://doi.org/10.1595/205651325X17375408788409

[39] M. Gundagani, V. Javvaji, D. Gadipalli, et al. A numerical study on MHD 3-D Casson-nanofluid flow past an exponentially stretching sheet with double Cattaneo-Christov diffusion effects. *Revista Internacional de Métodos Numéricos para Cálculo y Diseño en Ingeniería* **41**(2):21, 2025. https://doi.org/10.23967/j.rimni.2025.10.63195

[40] M. Gundagani, T. K. Tak, S. B. Krishnan, et al. Hall current and ion slip effects on 3D MHD nanofluid flow of Eyring-Powell fluid with gyrotactic microorganisms. *Advances in Systems Science and Applications* **2024**(4):9–27, 2024. https://doi.org/10.25728/assa.2024.2024.4.1538

[41] B. R. Nagasmitha, V. Nagendramma, N. Ahmed, et al. Analytical study of nonlinear behavior and convection patterns in Darcy-Brinkman porous medium with Maxwell-Cattaneo ferroconvection. *Journal of Mines, Metals and Fuels* **73**(2):437–445, 2025. https://doi.org/10.18311/jmmf/2025/47828

[42] F. Mebarek-Oudina, G. Dharmaiah, J. L. R. Prasad, et al. Thermal and flow dynamics of magnetohydrodynamic Burgers' fluid induced by a stretching cylinder with internal heat generation and absorption. *International Journal of Thermofluids* **25**:100986, 2025. https://doi.org/10.1016/j.ijft.2024.100986

[43] M. A. Kumar, F. Mebarek-Oudina, P. Mangathai, et al. The impact of soret dufour and radiation on the laminar flow of a rotating liquid past a porous plate via chemical reaction. *Modern Physics Letters B* **39**(10):2450458, 2025. https://doi.org/10.1142/S021798492450458X

[44] F. Mebarek-Oudina, M. Bouselsal, R. Djebali, et al. Thermal performance of MgO-SWCNT/water hybrid nanofluids in a zigzag walled cavity with differently shaped obstacles. *Modern Physics Letters B* **39**(29):2550163, 2025. https://doi.org/10.1142/S0217984925501635

[45] J. Raza, F. Mebarek-Oudina, H. Ali, I. E. Sarris. Slip effects on Casson nanofluid over a stretching sheet with activation energy: RSM analysis. *Frontiers in Heat and Mass Transfer* **22**(4):1017–1041, 2024. https://doi.org/10.32604/fhmt.2024.052749

[46] B. O. Said, F. Mebarek-Oudina, M. A. Medebber. Magneto-hydro-convective nanofluid flow in porous square enclosure. *Frontiers in Heat and Mass Transfer* **22**(5):1343–1360, 2024. https://doi.org/10.32604/fhmt.2024.054164

[47] K. Ramesh, F. Mebarek-Oudina, B. Souayeh (eds.). *Mathematical modelling of fluid dynamics and nanofluids*. CRC Press, 1st edn., 2023. https://doi.org/10.1201/9781003299608

[48] F. Mebarek-Oudina (ed.). *CFD simulation: Thermo-Fluids and nanofluids in engineering and biomedicine*. De Gruyter, Berlin, Boston, 2025. https://doi.org/10.1515/9783111405094

[49] A. Mezaache, F. Mebarek-Oudina, H. Vaidya, Y. Fouad. Heat transfer analysis of nanofluid flow with entropy generation in a corrugated heat exchanger channel partially filled with porous medium. *Heat Transfer* **53**(8):4625–4647, 2024. https://doi.org/10.1002/HTJ23149

[50] V. Makkar, P. Batra. Numerical simulation of MHD convective nanofluid flow with buoyancy forces over three dimensional exponential stretching surface. *Materials Today: Proceedings* **52**:810–817, 2022. https://doi.org/10.1016/j.matpr.2021.10.169